Int. J. Impact Engng Vol. 5, pp. 221–237, 1987
Printed in Great Britain

0734-743X/87 $3.00 + 0.00
Pergamon Journals Ltd.

V 392

HYPERVELOCITY IMPACT IN METALS, GLASS AND COMPOSITES

Burton G. Cour-Palais
NASA Lyndon B. Johnson Space Center
Houston, Texas 77058

ABSTRACT

This paper is a review of hypervelocity impact research carried out during the intense activity period leading up to the Apollo lunar missions. It is intended as a historical note on the research into hypervelocity impact phenomena in metallic, glass, and composite materials and the spacecraft applications of that research. The specific areas covered include cratering and spallation in thick, semi-infinite targets, perforation and hole formation in thin, single-thickness targets, spaced dual sheet armor, impact radiation, and impact ionization. Optimum and nonoptimum dual sheet combinations are treated in some detail because of the current interest in hypervelocity impact protection for the Space Station. On the other hand, the treatment of hypervelocity impacts on composites, phenolic resins and thermosetting epoxy systems reinforced with graphite or other high strength fibers, is limited because work in this area has just begun.

INTRODUCTION

Some twenty years after the Apollo designers had to contend with the unknown consequences of meteoroid impacts on manned spacecraft there is a new concern. A manmade orbiting debris population has been and is being added to the natural meteoroid environment and poses a threat to long-duration, long-term manned missions in near-Earth space (Kessler, 1981; 1982; 1985; Kessler and Cour-Palais, 1978). A sense of complacency seems to have pervaded the planners of new space operations after Skylab survived in Earth orbit without any penetration of the habitable volume for 6 years. However, there is now an awareness that the designers of new space ventures will have to contend with the consequences of rather poorly controlled littering of the near-Earth environment with dead spacecraft or fragments of spacecraft. Now that civilian and military space planners have begun to understand the problem, greater efforts to control the unnecessary littering of space is expected in the future.

The purpose of this paper is to provide some insight into the effect of hypervelocity impacts on spacecraft, the ability to take advantage of certain physical and dynamic aspects of an encounter with very high speed "projectiles" to minimize shielding, the nature of the threat that we are facing today, and the direction of the research being conducted in the civilian space arena. This includes a selective review of the pertinent work done by a number of investigators.

The Environment

What was the threat to manned space operations when President Kennedy set a national goal of landing a man on the Moon's surface by 1970? Very high speed solid particles, or meteoroids, had been observed as "meteors" in the atmosphere from the beginning of recorded history. Those that survived atmospheric ablation and were recovered as "meteorites" were broadly classified as stones or irons. This meant that some of the impacting particles could have a high mass density and could be more penetrating than similar mass low-density meteoroids.

Scientific observations of meteors began in the United States in 1911 with visual observations by the American Meteor Society (McKinley, 1961). McKinley states that the modern technique of photographic observations was initiated by Whipple in the 1930's as part of the Harvard Observatory's regular night sky patrol program. The two modifications that enhanced the value of

photographic records for meteor work were the rotating shutter placed in front of the lens and the mounting of two cameras 38 km apart directed at the same sky area (Whipple, 1938). These two developments were used to determine the angular velocity and the path parameters of the meteors detected on the photographic plates (McKinley, 1961).

The advent of the Super-Schmidt camera, designed by James Baker of Harvard specifically for meteor work, led to an intense study of meteors by the Harvard group in New Mexico between March, 1952, and October, 1953 (Whipple, 1952, 1954, 1958). This work resulted in the determination of meteor influx rates as a function of photographic magnitude (Hawkins and Upton, 1958) and the calculation of a meteoroid velocity distribution relative to the Earth (Hawkins and Southworth, 1958; McCrosky, 1957). Other experimenters in Europe and Canada also determined meteor influx rates from visual and telescopic observations (McKinley, 1961).

Relationships between the observed meteor magnitudes and the corresponding in-space meteoroid masses were required before a design meteoroid mass distribution could be derived. McKinley (1961) covers the attempts by Whipple, Opik, and others to derive an acceptable value for the mass of a zero magnitude meteoroid, which was a derivative of the assigned mass density. The mass density of most of the photographic meteors was assumed to be under 1 g/cm^3 due to the evidence of fragmentation high in the atmosphere (Jacchia, 1955).

It was apparent from the available mass distributions that the photographic and visual meteoroids were not a problem to the Apollo missions due to the very low probability of a damaging impact. However, it was known that meteoroids that did not leave a luminous trail in the atmosphere could be detected by radar and that these were far more numerous (McKinley, 1961). Also, the direct measurement of meteoroid impacts by satellites with various types of detectors had become a viable option (Alexander and colleagues, 1963). These results also showed that there were many more potentially damaging particles in space than had been detected by either the photographic records or the ground-based radar observations.

Under the impetus of the Apollo Program, the necessary radar and satellite measurements were made (Clifton and Naumann, 1966; Elford, 1967; Hastings, 1964; Hawkins, 1963; McKinley, 1961; O'Neal, 1968) and a design meteoroid environment model was derived for the Apollo Program in consultation with Whipple and the other experimenters at the Smithsonian Astrophysical Observatory and the NASA Centers (Cour-Palais, 1969a). This design environment model specified an Earth-centered velocity distribution which had an average of 20 km/s, a mass density of 0.5g/cm^3, consistent with the observations of meteoroid fragmentation in the upper atmosphere as reported by Jacchia (1955), and a cumulative distribution of masses between a gram and a nanogram. The distribution for the gram to microgram range is expressed in logarithmic form as

$$\log N = -14.37 - 1.21 \log m \qquad (1)$$

where N is the integrated flux of particles passing through one side of a square meter area every second, and m is the mass of the particle in grams.

The flux of particles between a microgram and a nanogram with the same units is

$$\log N = -14.34 - 1.58 \log m - 0.06(\log m)^2 \qquad (2)$$

Several other environment models of the meteoroid population in the Earth-Moon region of space have been formulated as the result of investigations of the returned lunar samples and spacecraft measurements since the end of the Apollo Program.

The orbital debris environment has had a similar history. Ground-based radar observations have catalogued Earth-orbiting objects to a limiting diameter of about 10 cm at an altitude of 1000 km (Kessler, 1981; Kessler and Cour-Palais, 1978). Taff and his colleagues (1985) report that they have been able to discriminate debris fragments as small as 1 cm with their electro-optical system, and impacts observed on spacecraft have confirmed the presence of debris with particle diameters in the micrometer to the sub-millimeter range (Kessler, 1985). Intermediate sizes have not been confirmed, but they are expected to exist based on laboratory hypervelocity tests. Sufficient information is available, however, to provide designers with a reasonably secure model of the cumulative number versus size distribution of the near-Earth orbital debris for diameters ranging from about 10 meters to a tenth of a millimeter (Kessler, 1982). The average collision velocities between a spacecraft in 30 and 60 degree inclination near-Earth orbits and orbiting debris fragments are 10 and 14 km/s, respectively (Kessler, 1982). Kessler states that these high speeds are a result of the concentration of debris at these and higher latitudes and the rapid precession of their ascending nodes (Kessler and Cour-Palais, 1978). The average mass density of debris fragments 1 cm and smaller in diameter is expected to be that of aluminum, 2.78 g/cm^3.

Impact Damage in Metallic Targets

Thick targets. The damage apparent to the block of aluminum depicted in Fig. 1 dramatically demonstrates the damage that results from a hypervelocity impact into a solid, metallic target. What is seen is a section through the crater and rear surface spall produced by a polyethylene projectile, like the one shown on the base of the stand, impacting a block of 1100-0 aluminum alloy at 7 km/s. The target was impacted at the GM Defense Research Laboratories, now Delco, at Santa Barbara, California, during the 1960's. What is seen is a nearly hemispherical, smooth crater with a raised lip on the front surface. This is typical of the hydrodynamic phase of a very high speed impact, when the impact pressure exceeds the strength of the target material. If the block had been made of a more brittle material, the lip would have been missing and the crater less smooth.

Other typical features of a hypervelocity impact on a solid target are seen at the other end of the target. The most prominent of these are the almost detached spalls from the back and top sides. Spallation is the result of the block not being thick enough to be "semi-infinite", that is, the reflected tensile stress wave from the rear free surface is still higher than the critical normal fracture stress (Rinehart and Pearson, 1963). A target can be considered to be semi-infinite when the rear surface is just on the point of separation. In this target, we see that the projectile hit off the center of the block; the top edge has started to spall, but the bottom edge has not. Another interesting feature of this target is the corner cracking at 45 degrees. This is brought about by the resultant stress caused by the meeting of two reflected tensile stresses from the free surfaces of the block. Notice that at the bottom of the block the crack can occur without the spall.

The size and impact energies of the meteoroids most likely to be encountered during the Apollo missions were simulated by launching particles ranging from 1.27 cm to 50 μm in diameter at hypervelocities. Typical two-stage light-gas gun velocities for projectiles between 0.16 cm and 1.27 cm were from about 6 to nearly 9 km/s (Denardo, Nysmith, and Summers, 1967; Goodman and Liles, 1963; Halperson, 1963). However, the 50 μm projectiles could be accelerated to between 12 and 18 km/s using an electro-thermal gun (Scully and colleagues, 1965).

According to Gehring (1970b) it was well established that crater shapes tended to be hemispherical in the hypervelocity regime and that the crater dimensions scaled linearly with the projectile diameter for any velocity. Figure 2 is a plot of the projectile diameter to crater depth ratio, p/d, as a function of the impact velocity V in km/s, for spheres ranging from 50 μm to 1.2 cm. It is apparent that the 50 μm data falls below the other projectile results. The validity of this effect was confirmed by the author of this report by plotting the projectile diameter as a function of p/d for three widely separated pyrex glass sphere sizes, 0.635 cm, 0.4 mm, and 50 μm impacting a 2024-T4 target at 7 km/s. It was found that the p/d scaled as the 19/18 power of the projectile diameter for this velocity and for these projectile and target materials. If the results of Fig. 2 are replotted with the projectile diameter raised to the 19/18 power, as shown in Fig. 3, all the data points are in much better agreement. This size scaling factor was discussed with Maiden (1964) who felt that the nonlinearity must apply to the strength dependent phase of the cratering process, as the crater to diameter ratio must be linear during the hydrodynamic phase.

Fig. 1. Sectioned hypervelocity impact crater and spallation in a 1100-0 aluminum block.

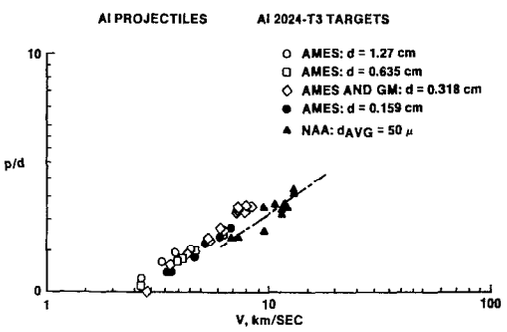

Fig. 2. Penetration depth to projectile diameter ratio as a function of velocity without diameter scaling.

While investigating the momentum transfer associated with the hypervelocity impact of aluminum spheres into thick aluminum targets at velocities up to 7.3 km/s, Denardo and Nysmith (1964), found that a correction factor using the projectile diameter raised to the 1/18 power improved the correlation of the crater depths and diameters.

Denardo, Summers, and Nysmith (1967) reported the results of a detailed experimental investigation of this phenomenon with projectiles ranging between 1.27 cm and 0.16 cm at impact velocities up to 8.5 km/s. They concluded that the agreement between macroparticle and microparticle penetration, with allowance for the 1/18 power law for diameter scaling, was remarkable for the velocity range that they tested. They further stated that in conjunction with the results obtained by Slattery and Friichtenicht (1966), with hypervelocity microparticle impacts into 1100-0 aluminum targets, the 1/18 scaling law extended over a diameter range of four orders of magnitude. This was significant because it allowed the higher speed data available for the small projectiles to be used to extend the results obtained for the larger, relatively slower ones.

The size scale factor was later shown by Gault and Moore (1965) to be related to the rupture stress and mean deformation strength of the target material. They stated that the exponent of the projectile diameter varies between 1.2 for very brittle materials such as rock and glass to nearly one for a ductile aluminum alloy. Subsequent analytical studies (Riney and Heyda, 1964; Rosenblatt, 1970; Sedgwick, 1966) showed that this nonlinear scaling phenomenon could be accounted for by the inclusion of material strain-rate and incipient melting effects in their numerical descriptions of the impact process. Diameter scaling remains an important factor in the comparison and the extrapolation of test data over a significant size range.

The strength and ductility of the target material also influence the final dimension of the crater in a semi-infinite target. In Fig. 4 the penetration depth to projectile diameter ratio, with size scaling, is plotted as a function of velocity for two aluminum alloys, 1100-0 and 2024-T3. The 1100-0 is a very soft, ductile material with a Brinell Hardness Number of 27. The 2024-T3 is harder and less ductile, and its Brinell Hardness number is 145. A comparison of the laboratory data from two different sources in Fig. 4 shows that the difference in the depth to diameter ratio is distinct, and the reasons for this are understood (Holsapple and Schmidt, 1982; Meyers and Charest, 1964; Prater, 1970). As mentioned previously, the initial shock pressure during a hypervelocity impact is high enough to cause the target material to behave as a fluid. Crater growth during this phase is identical for the hard as well as the soft aluminum alloy, because their relative strengths are not important. As the shock pressure decays and the material properties begin to dominate again, the crater dimensions are eventually "frozen" at different times for the two alloys. To illustrate this, the 1100-0 alloy has a yield stress of $4.4 \times 10^{10}\ N/m^2$ and an ultimate strength of $8.96 \times 10^{10}\ N/m^2$. The comparable values for the 2024-T3 are $2.48 \times 10^{11}\ N/m^2$ and $3.31 \times 10^{11}\ Nm^2$, respectively. For a given impact shock pressure and similar decay characteristics, the 2024-T3 crater will stop growing before the 1100-0 crater. According to Meyers and Charest (1964) the 2024-T3 crater growth limitation begins at 21 μs after impact, whereas the 1100-0 crater continues for another 16 μs. The same authors also state that the final crater dimensions for the 1100-0 case can be as much as 15% less than the maximum achieved during the impact process. This rebound effect is probably more noticeable for the ductile materials and is a transient event that can only be detected by x-radiography.

Several empirical hypervelocity equations describing crater formation in semi-infinite metallic targets were derived during the Apollo era (Herrmann and Jones, 1961; Herrmann and Wilbeck, 1986;

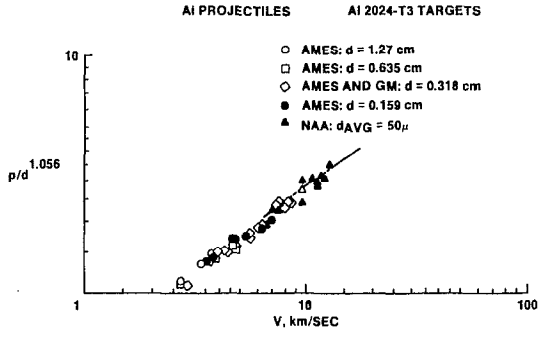

Fig. 3. Penetration depth to projectile diameter ratio as a function of velocity with diameter scaling.

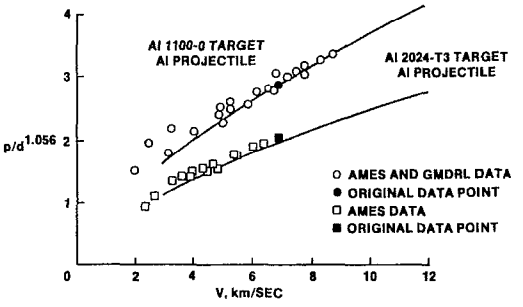

Fig. 4 Penetration depth to projectile diameter ratio as a function of velocity with diameter scaling and material strength effects.

Wenzel and Gehring, 1965). Gehring (1970b) discusses two of these equations and describes some of the fundamentals involved in deriving practical cratering equations. Empirical equations are considered valid only a few kilometers per second beyond the limits of the hypervelocity test data used for their derivation. Extrapolation to meteoroid or orbital debris velocities depended on the results obtained from numerical calculations based on an understanding of the impact process (Bjork, Kreyenhagen, and Wagner, 1967; Dienes and Walsh, 1970; Riney, 1964; Rosenblatt, 1970; Wagner, Brooks, and Bjork, 1965; Walsh and Johnson, 1965). For the average debris encounter velocity, 10 km/s, for a spacecraft in a 30 degree inclination orbit, little or no extrapolation is necessary.

Experimental results at the highest light-gas gun speeds attained in the laboratory favored a velocity scaling to the 2/3 power (Halperson, 1963; Sorensen, 1965; Wenzel and Gehring, 1965). Numerical analyses by Walsh and his colleagues (1964, 1965) showed that the crater dimensions increased as the 0.58 power of the impact velocity for velocities that were greater than about twice the target sound speed. However, Riney and Heyda (1964) concluded that the depth of penetration in a thick target varies with the impact velocity to the 2/3 power in the hypervelocity regime. Both groups agreed that there was no effect of projectile density on the crater dimensions at constant mass, provided that the target and projectile densities differed by no more than a factor of three. They also found that the target strength played an important role in limiting the crater size at all hypervelocity levels.

Light-gas gun hypervelocity test results, plotted as p/d as a function of velocity, could not differentiate between the 0.58 and 2/3 velocity scaling (Halperson, 1963; Wenzel and Gehring, 1965). Wenzel and Gehring also show comparisons between shaped charge hypervelocity test results to 16.3 km/s and the same two velocity power law dependencies, but again without clearly settling the issue. The empirical equation, given by Wenzel and Gehring (1965) in which the penetration depth in a semi-infinite target is proportional to the 1/3 power of the impact energy, correlates well with the shaped-charge data to over 16 km/s. Kineke (1965), using impact data obtained by various explosive devices to 12 km/s with steel, aluminum, and titanium projectiles and copper and lead targets, finds good correlation with velocity scaling to 0.58.

Recent investigations of the existing theoretical and empirical scaling laws for cratering phenomena by Holsapple and Schmidt (1980, 1982), originally concerned with large terrestrial and planetery craters where gravity and strength are very significant factors, have led to a better understanding of scaling in general. They show that scaling laws are more complicated than the preceding discussion might imply and that energy scaling, momentum scaling, strength scaling, and gravity scaling are points on an envelope of permissible scaling rules.

Thin or plate targets (less than semi-infinite). Up to this point, the discussion has been about semi-infinite targets. If the target is made progressively thinner and if the projectile mass and velocity are kept constant, a piece of the rear surface will spall as can be seen in Fig. 1. The size and cohesiveness of the spall depends on the material properties, as well as the strength of the shock as it reaches the rear surface of the target. Further reduction of the target thickness will result in the crater and the spall meeting, and the target is perforated. Since it is more often necessary in aerospace applications to assess the penetration resistance of targets that are much thinner than semi-infinite, "finite thickness" equations were needed. The first approach was to determine empirical finite thickness factors, applicable to varying degrees of spallation, to be applied with the crater depth equation (Gehring, 1970b). The spall factors reported by Gehring were for 2024-T3 aluminum alloy targets impacted by 0.32 cm diameter aluminum projectiles at a nearly constant velocity of 7.4 km/s. Spallation began to occur at a thickness of three times the crater depth and broke away when the thickness of the target was about 2.3 times the crater depth. Perforation resulted when the thickness was only 1.8 times the crater depth.

Although these factors were determined for a specific brittle aluminum alloy, they were used for other aluminum alloys with similar properties. The point is that finite thickness equations were not formulated early in the Apollo Program, and the procedure of applying spall factors to cratering equations was fairly standard procedure, until Fish and Summers (1965) determined the perforation limit of a number of materials used in satellite meteoroid impact detectors. These authors defined this limit as the velocity at which a given target was damaged to the point that it could not sustain a pressure differential of $1 \times 10^5\ N/m^2$ without leaking. The tests were performed with 0.16 cm aluminum projectiles at hypervelocities up to 8.5 km/s, and they found that the perforation limit varied inversely with the square root of the density of the target material and the 1/18 power of its ductility. The Fish-Summers perforation formula is usually written in a more convenient form (Frost, 1970; Naumann and Jex, 1969) as follows

$$t = K \times (\rho)^{0.148} \times (m)^{0.352} \times (V)^{0.875} \qquad (3)$$

in which the units are V in km/s, m in g, ρ in g/cm^3, and K is a constant for the material calculated from its elongation, expressed as a percentage, and mass density. Values for K for

some of the more commonly used spacecraft and satellite penetration materials are given by Naumann and Jex (1969) and Frost (1970). For aluminum 2024 alloy in the T3 condition, K is 0.54, and for the annealed aluminum alloy 1100-0, K is given as 0.52.

Naumann and Jex (1969) calibrated the Explorer 23 and Pegasus meteoroid satellite impact detectors made from 0.0025 and 0.005 cm stainless steel, and 0.023 and 0.041 cm aluminum, respectively, using 24 to 33 μm borosilicate projectiles accelerated to 18 km/s in an electro-thermal gun facility (Scully and colleagues, 1965), and 40 to 200 μm borosilicate and plastic projectiles to 8 km/s using light-gas guns. They concluded that the Fish-Summers equation could not be extrapolated to very thin, metallic materials, because the perforation mechanisms were different than those normally seen in the thicker materials. Naumann and Jex (1969) mentioned that in several instances the crater depths exceeded the thickness of the sheet, indicating that the material had been drawn in the impact process.

Thin sheet spaced targets. Although there are many instances in which spacecraft structures can be adequately protected by a single thickness of material against hypervelocity impact, weight considerations usually prevent such protection. The principle of placing a thin sheet out in front of the main structural wall as a "bumper" was well known before the Apollo Program began, having been first suggested by the noted astrophysicist Whipple (1946, 1952). The initial tests on spaced targets confirmed that as a defense against hypervelocity impacts, a structure consisting of two thin sheets was significantly lighter and better than a single thickness of material.

During the early days of practical shielding design, it was necessary to arrive at the total thickness of a dual-sheet combination by comparing it with the equivalent single sheet or plate thickness. Hypervelocity tests had determined these equivalences for the same "ballistic limit" (Nysmith and Summers, 1962). The ballistic limit was defined by these authors as the velocity required to cause perforations resulting in a loss of pressure with a differential of 10^5 N/m^2. Nysmith and Summers (1962) tested several dual-sheet combinations at hypervelocities, varying the thicknesses, spacing, and materials, and later Nysmith (1968) updated and extended this work to 8.8 km/s. Posever and Scully (1965) investigated dual-sheet configurations of aluminum alloy 5052-0 foils, 0.013 to 0.13 mm thick, using their electro-thermal gun facility. They obtained over 2700 data points with 50 to 75 μm borosilicate projectiles impacting at 15 to 18 km/s.

A large amount of research was done on the effects of varying bumper materials and thicknesses on the damage to the second sheet of a dual-wall configuration, and the properties required for the optimum performance of the bumper were identified (Gehring, 1970a; Maiden, McMillan, and Sennett, 1965; Meyers and Charest, 1964; Swift and Hopkins, 1969). The factors involved in the formation of the hole in the bumper were also studied (Nysmith and Summers, 1962; Swift and colleagues, 1969; Turpin and Carson, 1970), and several empirical equations were developed (Carey, McDonnell, and Dixon, 1985; Gehring, 1970a; Nysmith, 1968; Nysmith and Denardo, 1969; Sawle, 1969). The hole diameter equations (Herrmann and Wilbeck, 1986) included parameters such as the impact velocity, sheet thickness, and projectile diameter, and material terms such as density, strength, and shock properties for the projectile and the target. Comparisons of some of these equations with data are given by Turpin and Carson (1970) for typical spacecraft sheet thicknesses and by Carey, McDonnell, and Dixon (1985) for foil thicknesses.

Phenomenological approaches for sizing the elements of multielement meteoroid protection, in which the elements were dealt with separately, made it possible to optimize the beneficial properties of the bumper, the spacecraft shell or second sheet, and the spacing between them (Cour-Palais, 1969; Gehring, 1970a; Maiden, McMillan, and Sennett, 1965; Richardson, 1969; Swift and colleagues, 1982; Wilkinson, 1968; Woodall, 1967). Because dual or multisheet protection for space vehicles is still the most effective passive defense against hypervelocity projectiles, a discussion of some of the principles involved follows.

The outer wall, generally known as the "bumper" or shield, is the key element, and it determines the condition of the projectile after initial impact. When a metallic target subjected to hypervelocity impact is made progressively thinner to the point at which complete penetration occurs, an expanding cloud of projectile and target material is generated. This cloud can consist of solid, liquid, or vaporized material, or a combination of all three, depending on the initial impact pressure.

Figure 5 shows the results of an aluminum-aluminum impact by a 0.95 cm projectile at nearly 7 km/s, with an initial impact pressure of approximately 10^{11} N/m^2. On the right is a view of a 0.16 cm shield with an intact projectile on it for scale. On the left is the front surface of the second plate which was spaced 30.5 cm behind the shield. The brightness of the impact zone shows that the material was in the liquid state. The surface is roughened by multiple small craters in the central zone, and their density falls off with distance from the center of impact. Also, there is a radial pattern with strings of very small craters. All of these effects are a result of the remains of the projectile and of the shield hole material, and they illustrate rather dramatically how the shield works. The impact of the debris cloud on the second or backup

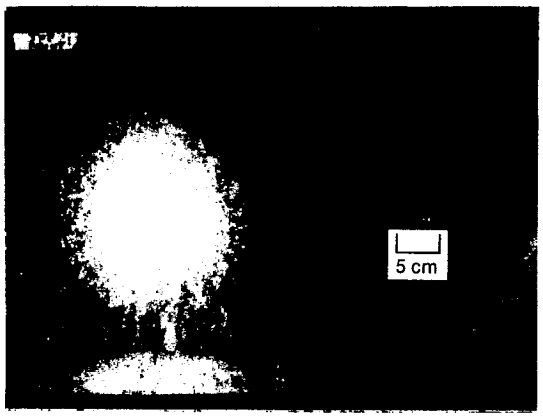

Fig. 5. Characteristic hypervelocity impact damage patterns for dual-sheet configurations: surface damage with no penetration.

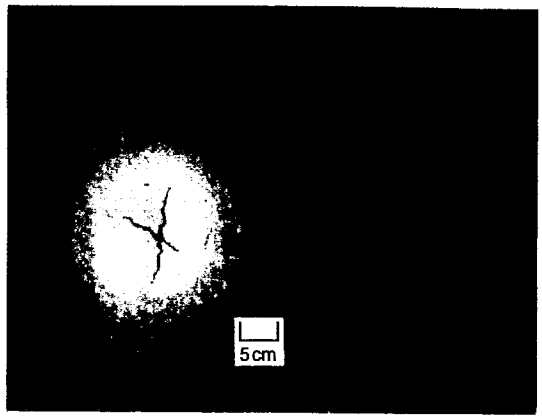

Fig. 6. Characteristic hypervelocity impact damage patterns for dual-sheet configurations: rupture, front view.

sheet can result in various types of damage. In the case shown in Fig. 5, the damage is superficial because the backup sheet is too thick to be efficient. If it had been thinner, there would have been spall off the rear surface.

The next stage in the dual-sheet interaction with a hypervelocity projectile is illustrated in Fig. 6. With the same projectile, velocity, and spacing, the backup sheet has experienced a pre-petalling or rupture failure. The wall thickness was reduced to the point at which it could not withstand the impulse generated by the debris from the shield, and it split. The rear of this same plate is seen in Fig. 7, which shows the deep drawing of the material that preceded the split. Obviously, the ultimate tensile allowable and ductility play a large part in minimizing this type of failure. Another interesting phenomenon, seen in Fig. 6, is the aluminum vapor deposit on the rear surface of the front sheet. The secondary impact of the molten debris from the bumper interaction, at 80 to 90% of the initial projectile velocity (Swift and colleagues, 1969), is sufficient to exceed the vaporization temperature of aluminum. The vapor cloud is reflected from the front of the second sheet onto the rear of the front one, coating it in the process.

Figure 8 shows yet another type of failure in which the second sheet is perforated by numerous small crater and spall combinations. The front surface is easily recognized by the familiar bright, molten splatter from the bumper. In this case, the only variation from the target shown in Fig. 7 was that the bumper thickness was tripled. Other illustrations of second-sheet failure and some excellent time-resolved photography of the shield debris and its interaction with the second sheet are given by Swift and Hopkins (1969) and Gehring (1970a).

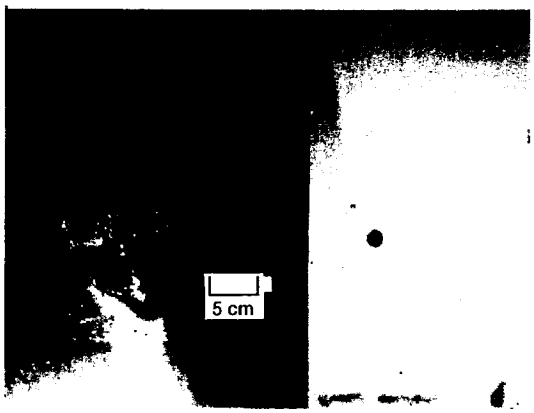

Fig. 7. Characteristic hypervelocity impact damage patterns for dual-sheet configurations: rupture, back view.

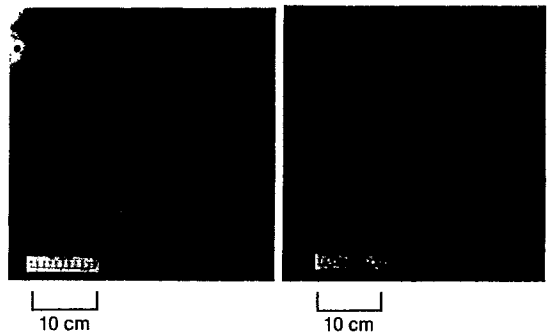

Fig. 8. Characteristic hypervelocity impact damage patterns for dual-sheet configurations: perforations.

The reaction of the second sheet of a dual-sheet configuration is, as has been mentioned, conditioned by the state of the debris from the projectile-bumper interaction. Gehring (1970a) summarized the work done by the General Motors group during the 1960's on the response of the second sheet to an optimum impact situation, which was achieved by using cadmium projectiles impacting cadmium shields at 6.5 km/s. The momentum imparted to the second sheet was measured and modelled, and an equation derived to determine the second-sheet thickness for fracture and yielding. The thickness, t_b, of the second sheet may be calculated from the equation

$$t_b = C \times (m \times V)/S^2 \tag{4}$$

where C = 41.5+ or -14 and 8.2+ or -1.4 for the 0.2% yield and fracture criteria for a 7075-T6 aluminum, respectively, t_b is in cm, V is the initial impact velocity in km/s, and S is the space between the bumper and the second sheet in cm. The 0.2% yield equation will give a sheet thickness that should not deflect or spall. On the other hand, the fracture criterion will result in a second sheet that may fail in tension, as depicted in Fig. 6.

When the projectile and shield are not in an optimum relationship, the second sheet is subjected to hypervelocity fragments from the shield and the molten residue of the projectile. Some of the nonoptimum projectile and shield combinations that result in more serious consequences to the second sheet are shown by Cour-Palais (1969b) and Gehring (1970b). Nonoptimum shield conditions are always the case for any dual-sheet configuration designed to operate in an environment with the size distributions previously described for the meteoroid and the orbital debris populations. The reason for this is that if a bumper is designed to be optimum for a particular design particle size, it is nonoptimum for both smaller and larger particle sizes. As the smaller particles are more numerous for either of the environments mentioned, the probability of penetration is higher than it was designed to be with an optimum bumper. Nonoptimum dual-sheet combinations were investigated by Cour-Palais (1969b, 1979), Gehring (1970b), and Swift and colleagues (1969), which resulted in various approaches to solving the problem, including qualification of a configuration by hypervelocity testing. Cour-Palais (1969) derived an empirical nonoptimum equation for the thickness of the second sheet, t_b, as follows

$$t_b = C \times m^{0.33} \times V/(S \times Y)^{0.5} \tag{5}$$

where C = 19.8 for projectiles up to 0.32 cm, m is the mass of the projectile before impact in g, V is the initial impact velocity in km/s, S is the space between the two sheets in cm, Y is the 0.2% yield stress of the second sheet material, and t_b is the required thickness in cm.

One way to depict the behavior of a dual-wall configuration subjected to hypervelocity impact is a plot such as Fig. 9 (Cour-Palais, 1969b, 1979; Gehring, 1970b; McMillan and colleagues 1966). The ratio of the sum of the shield thickness, t_s, and the backup thickness, t_b, to the projectile diameter is plotted as a function of the shield thickness to projectile diameter ratio. In Fig. 9 the data is for the aluminum alloy 7075-T6, a velocity of 7.4 km/s, a spacing of 5.08 cm, and 0.16 and 0.32 cm projectiles. The data at t_s/d zero correspond to a backup sheet without a bumper, and the value used for the calculated point is for a finite plate that is cratered and

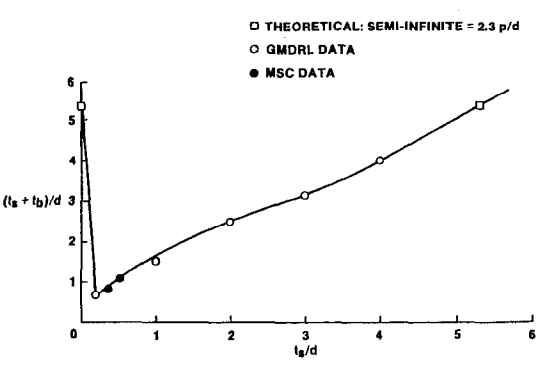

Fig. 9. Spectrum of nondimensionalized total thicknesses of spaced sheets required to prevent hypervelocity penetration, expressed as a function of shield thickness. The data refers to 7075-T6 aluminum sheets spaced 5.08 cm apart impacted at 7.4 km/s.

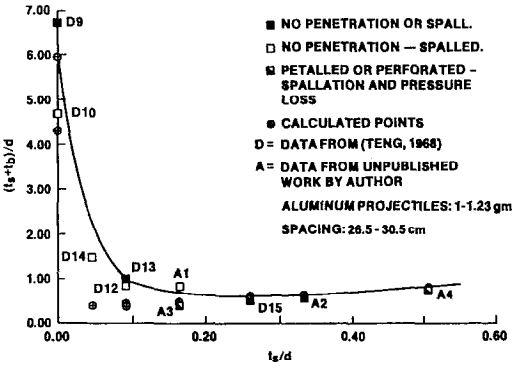

Fig. 10. Nondimensionalized total thicknesses of spaced sheets required to prevent hypervelocity penetration by 0.9 cm aluminum projectiles, for a limited range of shield thickness. The data refers to 2024-T3 aluminum sheets spaced 30 cm apart and impacted at approximately 7 km/s.

spalled but not penetrated. The thickness of the plate was calculated using a factor of 2.3 times the crater depth for the target condition described. As t_s/d increases, the total thickness decreases until it reaches a minimum at a t_s/d of about 0.15, which for this combination of projectile and target, is the optimum dual-sheet structure. Further increases in the ratio of shield thickness to projectile diameter is accompanied by an increase in the total thickness, as shown by the data points on the plot. The larger values of t_s/d, 1 through 4, are characterized by cratering and spall detachment from the rear surface of the bumper and fragments that can perforate the second wall (Gehring, 1970b). The plot in Fig. 9 is terminated at a value of t_s/d which corresponds to a shield which is thick enough by itself to prevent spall detachment, and consequently, the backup wall is unnecessary. Figure 9 illustrates the complete spectrum of effectiveness of the dual-sheet protection technique although it is only necessary to consider the minimum thickness portion of the curve such as is shown in Fig. 10. The data for Fig. 10 was obtained by the author for aluminum projectiles 0.88 and 0.95 cm diameter, impacting at approximately 7 km/s on two aluminum alloy 2024-T351 sheets spaced at 30 to 40 times the projectile diameter. The points marked A1, A3, and A4 are for the same targets shown in Figs. 5, 6, 7, and 8; A2 is an intermediate point with one small perforation and no penetration or spall. The other points marked "D" are data from an earlier series of tests (Teng, 1968) that represent other stages of the shield and backup interaction. The line through the data points divides the region between no penetration or rear surface spallation, and perforation or rupture leading to a loss of internal pressure. The points marked with crosses represent the calculated values for the borderline between the safe and the unsafe dual-wall protective structures, and although the plot is strictly valid between 4 km/s and 7 km/s, it can be used up to 10 km/s, the average debris impact velocity given previously in this paper. The calculated points correspond to the use of the nonoptimum backup thickness equation (5) with C = 31.75.

Figure 11 is a plot of the optimum shield thickness to projectile diameter as a function of velocity for an aluminum shield impacted by aluminum and glass projectiles. The solid line, reproduced from Maiden and his colleagues (1963, 1965), is the boundary between molten and solid projectile fragments, and the dashed line marks the melting threshold of the shield "hole". Aluminum is completely molten at an impact pressure of 0.88 $\times$ 10^{11} N/m^2 which occurs at 6.6 km/s for an aluminum on aluminum impact (Swift, 1982). The hole diameter equation given by Gehring (1970a) was used to calculate the amount of material to be melted, and the heat of fusion, Hf, was assumed to be 4% of the heat available in the impact. Data points in Fig. 11 were obtained by the author and are seen to agree with the projectile and shield melting thresholds. The open symbols are for aluminum projectiles, which left a bright splatter on the second sheet, and the solid symbols indicate results from glass projectiles impacting the aluminum shields. Glass projectiles were used because they exceed the melting impact pressure for aluminum at 7 km/s and allow the molten shield splatter to be clearly distinguished from the projectile. The zone between the solid and the dashed lines gives the range of t_s/d values for complete melting of the projectile and the shield. At laboratory light-gas gun speeds, and with projectiles up to 0.32 cm in diameter, the range of optimum t_s/d values is quite limited, but at the higher speeds there is a greater latitude for optimization. It is expected that the optimum zone will be much larger for the 1 cm projectiles as is noticeable in Fig. 10.

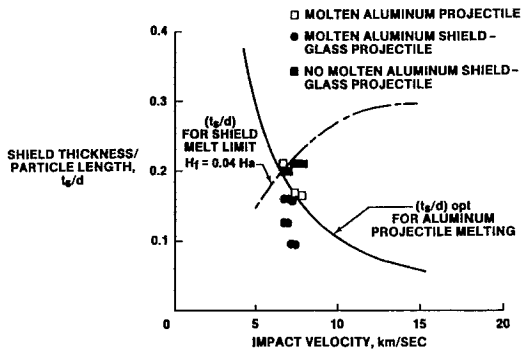

Fig. 11. Nondimensionalized limiting thickness of aluminum shields for complete melting of the projectile and shield plug material expressed as a function of impact velocity.

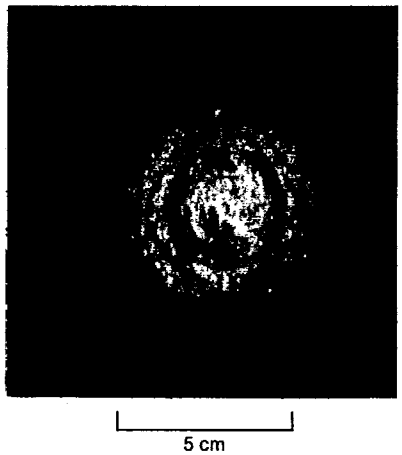

Fig. 12. Top view of hypervelocity impact damage in a fused silica (glass) target.

The previous discussion is applicable to hypervelocity impacts at right angles to the target. Most meteoroid and orbital debris impacts will be at angles between 30 and 50 degrees to the surface normal axis. McMillan and colleagues (1966) investigated oblique angle impacts into dual-wall, spaced targets at 30, 45, and 60 degrees and velocities in excess of 7 km/s. They found that unlike normal impacts at these speeds, the major source of damage was caused by fragments from the shield. The larger amount of discrete fragments can be expected because of the lower peak pressures associated with oblique impacts. McMillan and his colleagues state that the degree of fragmentation decreases as the angle from the normal is increased, with the greatest damage to the wall occurring at 45 degrees. Because the normal component of the impact velocity determines the initial impact pressure, the fragmentation problem will be lessened as projectile and target again achieve postimpact melting temperatures. This will begin to happen when the normal component of the velocity is above 7 km/s. It is expected that the zero degree impact total dual-wall thickness, as determined by a plot such as Fig. 11, will apply to the 30 to 45 degree case, if the normal component of the impact velocity is substituted.

It is very important to understand that the dual-wall configuration, capable of defeating a hypervelocity meteoroid or orbital debris particle, is vulnerable to projectiles that are not travelling fast enough to be broken up by the shield. Investigators of representative hypervelocity dual-wall combinations at speeds below 7 km/s (Gehring, 1970b; McMillan and colleagues, 1966) found that the maximum penetration effect, and consequently the thickest rear wall, occurred at about 2.5 km/s. In fact, the total thickness to prevent penetration at this velocity was the same as it would be for a 10 km/s impact for the same projectile diameter, although the failure mechanism would be different (Gehring, 1970b).

Impact Damage in Non-Metallic Targets

Glass targets. A hypervelocity impact in a thick glass target is far more dramatic than one into a block of metal. Although the initial impact pressure generated by a 7 km/s impact on glass is not much less than on aluminum, the damage is much more extensive. This is because of the brittle nature of all glasses and their low tensile strength, which allows the shock-related shear and release tensile stresses to dominate the material strength over a longer time. The damage is characterized by concentric rings of surface spallation which are progressively below the surface as the impact point is approached. This leads to a typically conical crater formation (Flaherty, 1969). The impact shown in Fig. 12 has these concentric zones well delineated in addition to other typical effects found in targets that are not semi-infinite. The concentric, discontinuous flaws are fracture zones within the glass caused by the reflected shocks off the free boundaries of the target. Notice also the radial cracks, which are most prominent at the corners.

The corner cracks are a feature of the target being too small for this particular impact, a 0.16 cm aluminum projectile at a velocity of about 7 km/s. The surface spall is between 6 and 7 cm in diameter, and the depth of the pit is 0.46 cm from the surface of the glass. The diameter to depth ratio is 13 to 15, and the surface spall is 40 to 45 projectile diameters. These are in sharp contrast to the impact damage in a brittle aluminum target, typically a pit depth of about 0.3 cm, and a surface spall ring only slightly larger than the pit diameter, which is about 4 projectile diameters. The target shown is 2 cm thick, and there is a considerable amount of rear surface spallation. A glass target must be much thicker than its aluminum counterpart to prevent rear spall. Flaherty (1969) studied the phenomenology of crater and flaw formation in glass caused by a range of impact velocities from very low speeds to hypervelocities. He also looked into the effect of subsequent thermal loads on crater morphology. Other investigators (Cour-Palais, 1982; McHugh and Richardson, 1971, 1974; Wenzel and Gehring, 1965) provided the crater formation equations and the design parameters required to prevent cracking and to prevent spallation off the rear surfaces for the Apollo Program.

The impact shown in Fig. 12 for a 0.15 cm projectile at 7 km/s has done a lot of damage to the glass target. Had this been an observation port, it would have been of very little further use. However, the projectile energy and surface impact energy can be low enough, about 1 erg and 0.3 to 0.35×10^{11} N/m^2, to cause a lipped pit, as was observed on micron-sized particle hypervelocity impacts in glass (Roy, Slattery and Friichtenicht, 1972). As the energy increases, the first spall is detached around the pit, and sometimes this is accompanied by the ejection of the pit lips. Eventually, the energy level is sufficient for the concentric spallation to develop and for the crater to be ejected, leaving either a blocky, fractured indentation, marked by a sharp change of slope from the surrounding spallation, or a fused remnant (Cour-Palais, 1973). An appreciation of the forces at work in a glass target impacted at hypervelocity may be obtained by an examination of Fig. 13. This is a view of a sectioned, laminated target made up of a stack of aluminum sheets bolted together to provide good surface contact without a mechanical bond. The impact was at about 7 km/s, and one can see the crater, the shock compression under it, and the rebound of the upper layers as the release wave overcame the compression and the tensile "strength" across the interface. The significance of this target is that is simulates the low tensile strength of glass and its inherent brittleness. As one looks at the

successive peeled-back layers of the target depicted in Fig. 13, it is easy to see how the concentric spall zones are formed. Finally, the crater is beginning to be ejected as it is carried upward by the deeper spallation. A top view of the same target is shown in Fig. 14, and it clearly shows the spall zones and the radial tearing that is analogous to the radial cracks in the glass target.

Composite targets. The fiber-reinforced, cured resins and epoxy systems known as "composites" that compete on a strength-weight-cost basis with the aluminum and magnesium alloys used in spacecraft did not exist twenty years ago. These materials became commercially available in the late 1970's, and they have been used extensively for aircraft applications. Their use for spacecraft has only recently become significant, and the Space Shuttle external tank and the Orbiter cargo bay doors are examples of the acceptance of these new materials for important aerospace applications.

The use of the composites primarily for military aircraft meant that the only impact testing done until very recently was at typical ordinance velocities. Military hypervelocity impact research into the relative merits of either composites or the aluminum alloys has not been available. As a result, NASA has undertaken to investigate the hypervelocity impact properties of composite materials because of its own needs.

The NASA research in progress involves the experimental and analytical description of crater formation and delamination in various fiber and resin or epoxy combinations, using projectiles ranging in diameter from 0.2 mm to 0.32 cm, at impact velocities from 3.5 to 9 km/s. The target variables include the fiber strengths, the fiber orientation in the layups, and the total laminate thickness. Only nylon and aluminum projectiles have been used in the tests up to this point, but other materials consistent with orbiting debris will be investigated.

Preliminary results of this program are reported in these proceedings by Yew (1986), and several photographs of sections taken through the postimpact target damage areas are given by the author. Because composites are laminated materials, the reaction to the passage of a strong shock is very similar to the laminated aluminum target previously discussed and shown in Figs. 13 and 14. Like the aluminum target, the cratering process in a composite material will cause front surface delamination and peeling under the action of the shearing forces. However, the extent of the peeling in the composites is very directional and very extensive (Yew, 1986). Also, the target depicted in Fig. 13 shows the shock compression in the aluminum layers, which can be compared with the discolored area under the crater in the sectioned 96 lamina plate shown in Yew's Fig. 15 (Yew, 1986). Both the aluminum laminate and the 96 lamina composite are semi-infinite; therefore, there is no rear surface spall detachment, although the 96 lamina composite does show the onset of spallation by discoloration. Another noticeable effect of a strong shock on a laminated composite is the formation of fractures in the laminations (Yew, 1986), which could be a problem if the expected structural loads are across the fracture planes.

The initial results of hypervelocity impacts on a limited sample of composite materials show that composites are good candidates for spacecraft applications exposed to the meteoroid or debris environment, although the potential weight advantage has not been quantified.

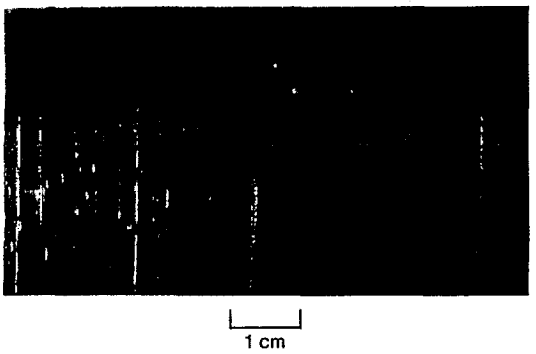

Fig. 13. Sectioned hypervelocity crater in a laminated aluminum sheet target.

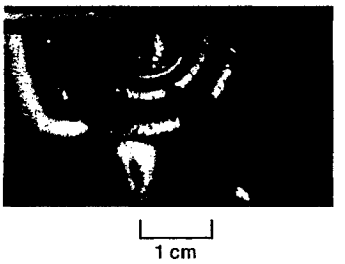

Fig. 14. Top view of sectioned crater in a laminated aluminum sheet target.

Impact Radiation and Ionization

Although the phenomenon most associated with hypervelocity impact is crater formation, there are two other effects that assumed some significance for their usefulness in the detection and identification of meteoroids. These phenomena are the flash of visible radiation and the ionization which are detectable at the instant of a high velocity particle impact (Eichhorn, 1976; Friichtenicht and Slattery, 1963; Gehring and Warnica, 1963; Jean, 1966; Jean and Rollins, 1969; MacCormack, 1963; Rosen and Scully, 1965). It may be of interest to discuss some of the experimental and analytical results of these investigations.

Jean and Rollins (1969) reported that they had isolated a narrow, fast-rising light pulse, followed by a much wider pulse which decayed slowly to zero intensity, in the impact flash. Typically, the time signature of the flash shows a spike with a half pulse width of 1 μs or smaller, and a rise time smaller than 0.2 μs followed by a slow-rising tail with a half pulse width of 3 to 5 μs. A specific example cited by these authors was for a 0.32 cm titanium projectile impact on a cadmium target at 3.5 km/s and a range pressure of 1.33×10^{-3} N/m^2. The spike height was 0.16 μs, its half pulse width was 0.5 μs, and the tail reached a maximum 3.4 μs after the onset of the spike. Jean and Rollins state that in some cases the spike and the tail merge and in others the spike is predominant and the tail very small.

Open shutter photographs such as Fig. 15 show the presence of two different light intensity levels corresponding to the two pulses that were observed. Time-resolved photographs, taken at 1 to 5.5 μs after the start of the spike, indicated that the tail of the impact flash was associated with the radiation emitted by an expanding, luminous, well-defined ring. The expansion velocity measured for the luminous ring produced by the 0.32 cm titanium sphere impacting the cadmium target at 3.5 km/s was 11.6 km/s. Other data presented by Jean and Rollins for aluminum-aluminum impacts also show that the ring expands at 2 to 3 times the projectile impact velocity.

The luminous spike was shown to be associated with the appearance of a "fast jet" of particles travelling at twice the speed of the luminous ring and detected by secondary targets at right angles to the main target. Jean and Rollins (1969) state that the fast jet and the luminous ring are produced by the same process at different pressures. These authors also show that the process that produces both the luminous spike and the tail is related to the production of a jet of material in a shaped charge. The angle between the tangent to the surface of a spherical projectile and the target at the impact interface, changes from 0 to 90 degrees during the penetration process. It passes through a critical angle for the formation of a jet which is akin to the critical angle in shaped-charge theory. The critical angle for the impact flash was measured using conical projectiles with different cone angles, and for copper-aluminum impacts, was found to range from 12.5 degrees at 1 km/s to 32 degrees at 6.3 km/s.

Jean and Rollins also conducted parametric studies of the flash to determine whether any of its characteristics could provide quantitative information about the size and velocity of the projectile. Copper spheres ranging in diameter from 0.16 to 0.64 cm were impacted into cadmium targets at 2 to 8 km/s, and only the impact spike measurements were used in the correlations. It was found that the peak intensity, I, of the radiation and the initial rate of change of the intensity, dI/dt, of the spike were strongly and consistently dependent on the diameter and

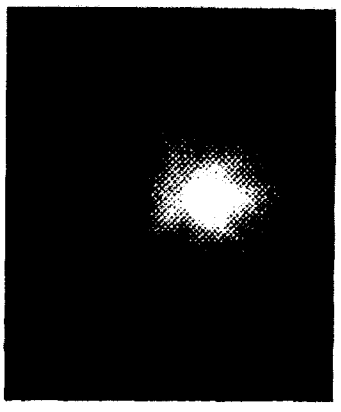

Fig. 15. Open shutter potograph of a typical impact flash.

velocity of the projectile for the chosen emission lines of cadmium: 5085, 3610, and 3261 Å. The measured peak intensity varied as the eighth power of the velocity for all three of the cadmium lines and the fourth power of the diameter at the 3610 Å transition for the copper projectiles. The rate of change of the spike intensity varied as the sixth power of the projectile velocity and approximately the square of the diameter for the same emission lines and projectile material and sizes.

Jean and Rollins also conducted spectrographic studies, using cadmium and aluminum targets and aluminum projectiles at 6 to 7 km/s with a range pressure between 1.33×10^3 to 1.33×10^4 N/m^2. They concluded that the short-duration, transient spike could be attributed to the presence of a hot, dense plasma at the impact point, while the long-duration tail was a result of the radiation of a neutral gas expanding from the impact zone.

Eichhorn (1976) continued the early research conducted by Jean and Rollins, performing his experiments with a 2 MV Van de Graaff dust accelerator. He confirmed that the mass and velocity dependence of the various parameters of the impact flash were suitable for the measurement of micrometeoroid impacts on spacecraft and gave the relationships for I, the light intensity, and E the total light energy as follows

$$I = C1 \times m \times V^{4.1} \tag{6}$$

$$E = C2 \times m \times V^{3.2} \tag{7}$$

where the units are m, the projectile mass in grams, g; V, the projectile velocity in km/s; $C1$ and $C2$ are constants depending on projectile and target material; I is in ergs/s; and E is in ergs.

Eichorn (1976) also found that impact flash measurements provided details about the crater-forming process. Using the spectral distribution of the light emission, he estimated the temperatures of the radiating gas and plasma. He was able to obtain the total thermal energy of the radiating gas and combine this with the estimated gas temperature to arrive at the total mass of the vapor produced during an impact. This led Eichorn to conclude that for iron particles impacting gold targets at 7.4 km/s, at least 1.6% of the displaced projectile and crater material was vaporized.

Spray particles at ejection angles less than 20 degrees were also detected by Eichorn (1976) for the iron particles impacting gold targets. He states that the velocity of this ejecta increased with primary velocity, but only up to 5 km/s, after which it remained practically constant. The maximum velocity measured by the author was 30 km/s for an initial particle impact at 4.8 km/s.

The impact ionization effect is the production of free charge at the site of a hypervelocity impact on a suitable target (Friichtenicht and Slattery, 1963). These authors did their research using micron-sized iron and graphite particles impacting targets of various materials at velocities up to 16 km/s in a 2 MV Van de Graaff accelerator. The impact creates temperatures high enough to vaporize the projectile and some of the target material and also to thermally ionize a fraction of the vaporized atoms. The result is a microplasma from which charge may be extracted through the application of electric fields (Becker and Slattery, 1972). Friichtenicht and Slattery (1963) state that the charge, Q, produced at impact is proportional to the mass of the projectile and the cube of the impact velocity and give the following relationship

$$Q = K \times E \times V/A \tag{8}$$

where Q is in coulombs; K is a quantity that contains target material properties; E is the particle energy in ergs; V is the particle velocity in km/s; and A is the atomic weight of the particle material.

Like the impact flash, the ionization charge signal shows two components for particle impacts under about 10 km/s. The first one follows immediately after the impact with an orgin that is close to the impact site. A second component is observed about 2 μs after the first, and its charge is collected on the target at some distance from the impact site (Becker and Slattery, 1972). These authors state that iron spheres less than 1 μm radius, impacting a solid surface at velocities less than 10 km/s, throw back small "spray" particles. The impacting particle is vaporized at this speed, and the charge produced per unit particle mass is approximately proportional to the fourth power of the impact velocity. This velocity dependence is the same reported by Jean and Rollins (1969) for the rate of change of flash intensity, as was mentioned previously in this report. The particles that impact at a velocity higher than 10 km/s are more completely vaporized, and produce either much smaller, or many fewer spray particles. Becker and Slattery (1972) feel it is these spray particles which create the delayed charge component, and they note that the earlier component of ionization is always present, but that the delayed charge component is only seen for velocities below 10 km/s. Jean and Rollins (1969) say that for the

similar case involving impact flash, there is no tail, or later component, at higher velocities because the amount of material produced is not enough to be excited. In conclusion, Becker and Slattery (1972) warned that particle velocity measurements based on the character of the impact ionization signal should be treated with great care.

Cosmic dust impact detectors, which made use of the ionization produced by an impact on a known target material, were designed and successfully flown on the Helios and Heos 2 spacecraft (Dietzel and colleagues, 1973; Grun and colleagues, 1980). The Helios 1 instrument had a sensitivity threshold of 3×10^{-16} kg at an impact speed of 10 km/s, and the measured parameters allowed the particle mass, speed, electrostatic charge, and composition of the plasma produced by an impact to be determined. Impact plasma detectors similar to the Heos 2 instrument were used on the European Space Agency's Giotto mission through the tail of Comet Halley and will be used on board the Ulysses mission, formerly ISPM, to detect interplanetary dust and measure its dynamic and physical properties (Grun and colleagues, 1983). The information available in the characteristics of an impact flash was never used for flight instrumentation, and this technique remains a valuable diagnostic tool for laboratory hypervelocity impact studies.

CONCLUSIONS

A historical overview of the research into the phenomenology of hypervelocity impact, especially as it relates to protection of spacecraft from meteoroid impacts during the manned Apollo Program, has been presented. The Apollo Program was the driver for a very concerted effort to understand not only the nature of the threat facing man's first venture away from his planet but also how to ensure his survival in a hostile meteoroid environment. A long hiatus in civilian hypervelocity impact research ensued after the successful completion of the manned missions to the Moon. This hiatus has now been broken with the onset of the Space Station design, and there has been a resumption of civilian research and development impact testing. Much that had been previously learned is still applicable, but new research is particularly required to investigate the hypervelocity properties of the composite materials. A partial bibliography of the hypervelocity impact papers that were used for the design and certification of the Apollo meteoroid protection is given in Cour-Palais (1982).

REFERENCES

Alexander, W. M., C. W. McCracken, L. Secretan, and O. Berg (1963). Review of direct measurements of interplanetary dust from satellites and probes. In W. Priester (Ed.), Space Research, 3rd ed. pp. 891-917.

Becker, D. G., and J. C. Slattery (1972). Investigation of high-speed phenomena. Report Number 16623-6005-RO-00, TRW Systems Group, California.

Bjork, R. L., K. N. Kreyenhagen, and M. H. Wagner (1967). Analytical study of impact effects as applied to the meteoroid hazard. NASA CR-757.

Carey, W. C., J. A. M. McDonnell, and D. G. Dixon (1985). An empirical penetration equation for thin films used in capture cells. In R. H. Giese and P. Lamy (Ed.), Properties and Interactions of Interplanetary Dust. pp. 131-136.

Clifton, K. S., and R. J. Naumann (1966). Pegasus satellite measurements of meteoroid penetration. NASA TM X-1316.

Cour-Palais, B. G. (1969a). Meteoroid environment model-1969 (near-Earth to lunar surface). NASA SP-8013.

Cour-Palais, B. G. (1969b). Meteoroid protection by multi-wall structures. Paper Number 69-372, AIAA Hypervelocity Impact Conference, Vol. of Technical Papers.

Cour-Palais, B. G. (1973). Apollo window meteoroid experiment. In Apollo 17 Preliminary Science Report, NASA SP-330, No. 21.

Cour-Palais, B. G. (1979). Space vehicle meteoroid shielding design. In N. Longdon (Ed.), The Comet Halley Micrometeoroid Hazard, ESA SP-153. European Space Agency, Paris. pp. 85-92.

Cour-Palais, B. G. (1982). Hypervelocity impact investigations and shielding experience related to Apollo and Skylab. In Orbital Debris, NASA Conf. Publication 2360. pp. 247-275.

Denardo, B. P., and C. R. Nysmith (1964). Momentum transfer and cratering phenomena associated with the impact of aluminum spheres into aluminum targets at 24,000 ft/s. Agardograph 87, Vol. 1.

Denardo, B. P., J. L. Summers, and C. R. Nysmith (1967). Projectile size effects on hypervelocity impact on craters in aluminum. NASA TN D-4067.

Dienes, J. K., and J. M. Walsh (1970). Theory of impact: some general principles and the method of eulerian codes. In R. Kinslow (Ed.), High-velocity Impact Phenomena. pp. 45-104.

Dietzel, H., G. Eichorn, H. Fechtig, E. Grun, H. J. Hoffmann, and J. Kissel (1973). The Heos 2 and Helios micrometeoroid experiments. J. Phys. E. Sci. Instrum., 6. p. 209.

Eichorn, G. (1976). Analysis of the hypervelocity impact process from impact flash measurements. Planet. Space Sci., 24. pp. 771-781.

Elford, W. G. (1967). The incidence of meteors on the Earth derived from radio observations. In G. Hawkins (Ed.), Meteors Orbits and Dust, NASA SP-135.
Fish, R. H., and J. L. Summers (1965). The effect of material properties on threshold penetration. In Proc. Seventh Hypervelocity Impact Symposium, Vol. 6. pp. 1-25.
Flaherty, R. E. (1969). Impact characteristics in fused silica. Paper Number 69-367, AIAA Hypervelocity Impact Conference, Vol. of Technical Papers.
Friichtenicht, J. F., and J. C. Slattery (1963). Ionization associated with hypervelocity impact. In Proc. Sixth Symposium on Hypervelocity Impact, Vol. 2. pp. 591-612.
Frost, V. C. (1970). Meteoroid damage assessment. NASA SP-8042.
Gault, D. E., and H. J. Moore (1965). Scaling relationships for microscale to megascale impact craters. In Proc. Seventh Hypervelocity Impact Symposium, Vol. 6. pp. 341-351.
Gehring, J. W. (1970a). Theory of impact on thin targets and shields and correlation with experiment. In R. Kinslow (Ed.), High Velocity Impact Phenomena. Academic Press, New York. pp. 105-156.
Gehring, J. W. (1970b). Engineering considerations in hypervelocity impact. In R. Kinslow (Ed.), High Velocity Impact Phenomena. Academic Press, New York. pp. 463-514.
Gehring, J. W., and R. L. Warnica (1963). An investigation of the phenomena of impact flash and its potential use as a hit detection and target discrimination technique. In Proc. Sixth Symposium on Hypervelocity Impact, Vol. 2. pp. 627-681.
Goodman, E. H., and C. D. Liles (1963). Particle-solid impact phenomena. In Proc. Sixth Symposium on Hypervelocity Impact, Vol. 2. pp. 543-576.
Grun, E., H. Fechtig, R. Giese, J. Kissel, L. Linkert, J. McDonnell, G. Morfill, G. Schwehm, and H. Zook (1983). The ISPM dust experiment. ESA SP-1050. European Space Agency, Paris.
Grun, E., N. Pailer, H. Fechtig, and J. Kissel (1980). Orbital and physical characteristics of micrometeoroids in the inner solar system as observed by Helios 1. Planet. Space Sci., 28. pp. 333-349.
Halperson, S. M. (1963). Some phenomena associated with impacts into aluminum. In Proc. Sixth Symposium on Hypervelocity Impact, Vol. 2. pp. 525-541.
Hastings, E. C. (1964). The Explorer 16 micrometeoroid satellite. NASA TM X-949, Supplement 3.
Hawkins, G. S. (1963). The Harvard radio meteor project. In Smithsonian Contributions to Astrophysics, Vol. 7. pp. 53-62.
Hawkins, G. S., and R. B. Southworth (1958). The statistics of meteors in the Earth's atmosphere. In Smithsonian Contributions to Astrophysics, Vol. 2. pp. 349-364.
Hawkins, G. S., and E. K. Upton (1958). The influx rate of meteors in the Earth's atmosphere. Astrophysical J., 128. pp. 727-735.
Herrmann, W., and A. H. Jones (1961). Correlation of hypervelocity impact data. In Proc. Fifth Hypervelocity Impact Symposium.
Herrmann, W., and J. Wilbeck (1986). Review of hypervelocity penetration theories. In Intern. J. Impact Eng., Vol. 5.
Holsapple, K. A., and R. M. Schmidt (1980). On the scaling of crater dimensions, 1, Explosive processes. J. Geophys. Res., 85(B12). pp. 7247-7256.
Holsapple, K. A., and R. M. Schmidt (1982). On the scaling of crater dimensions, 2, Impact processes. J. Geophys. Res., 87(B3). pp. 1849-1870.
Jacchia, L. G. (1955). The physical theory of meteors No. 8: Fragmentation as a cause of the faint meteor anomaly. Astrophys. J., 121. pp. 521-527.
Jean, B. (1966). Experimental observations of optical radiation associated with hypervelocity impact. AIAA J. pp. 4-10.
Jean, B., and T. L. Rollins (1969). Radiation from hypervelocity impact generated plasma. Paper Number 69-364, AIAA Hypervelocity Impact Conference, Vol. of Technical Papers.
Kessler, D. J. (1981). Sources of orbital debris and the projected environment for future spacecraft. J. Spacecraft and Rockets, Vol. 18, 4. pp. 357-360.
Kessler, D. J. (1982). Proposed preliminary design criteria: model environment for the 1990's. In D. Kessler and S. Su (Ed.), Orbital Debris, NASA Conf. Publication 2360. pp. 79-83.
Kessler, D. J. (1985). Orbital debris issues. In Space Debris, Asteroids and Satellite Orbits, Advances in Space Research, Vol. 5, Number 2. Pergamon Press, Oxford. pp. 3-10.
Kessler, D. J., and B. G. Cour-Palais (1978). Collision frequency of artificial satellites: the creation of a debris belt. J. Geophys. Res., 83(A6). pp. 2637-2646.
Kineke, J. H. (1965). Hypervelocity impact: dependence of crater dimensions on impact velocity. Memorandum Report Number 1652. Ballistic Research Laboratories, Maryland.
MacCormack, R. W. (1963). Investigation of impact flash at low ambient pressures. In Proc. Sixth Symposium on Hypervelocity Impact, Vol. 2. pp. 613-625.
McCrosky, R. E. (1957). A rapid graphical method of meteor trail reduction. Smithsonian Contributions to Astrophysics, 1. pp. 215-224.
McHugh, A. H., and A. J. Richardson (1971). Glass equations for solar cells. J. Spacecraft and Rockets, Vol. 8, 6.
McHugh, A. H., and A. J. Richardson (1974). Hypervelocity impact damage to glass. STR 241. Rockwell International, Space Division, Downey, California.
McKinley, D. W. R. (1961). Meteor Science and Engineering. McGraw-Hill, New York.

McMillan, A. R., A. H. Jones, K. H. Meyer, B. L. Lathrop, C. J. Maiden, and R. E. Sennett (1966). Experimental investigations of simulated meteoroid damage to various spacecraft structures. TR66-67. GM Defense Research Laboratories, Santa Barbara, California.

Maiden, C. J. (1963). Experimental and theoretical results concerning the protective ability of a thin shield against hypervelocity projectiles. In Proc. Sixth Symposium on Hypervelocity Impact, Vol. 3. pp. 69-156.

Maiden, C. J. (1964). Private Communication.

Maiden, C. J., J. W. Gehring, and A. R. McMillan (1963). Investigation of fundamental mechanism of damage to thin targets by hypervelocity projectiles. TR63-225. GM Defense Research Laboratories, Santa Barbara, California.

Maiden, C. J., A. R. McMillan, and R. E. Sennett (1965). Thin sheet impact. In Proc. Seventh Hypervelocity Impact Symposium, Vol. 4. pp. 63-123.

Meyers, C. L., and J. A. Charest (1964). Research on the properties of optimum meteoroid shields. TR64-48. GM Defense Research Laboratories, Santa Barbara, California.

Naumann, R. J., and D. W. Jex (1969). Calibration of Pegasus and Explorer 23 detector panels. NASA TR R-321.

Nysmith, C. R. (1968). Penetration resistance of double-sheet structures at velocities to 8.8 km/s. NASA TN D-4568.

Nysmith, C. R., and B. P. Denardo (1969). Experimental investigation of the momentum transfer associated with impact into thin aluminum targets. NASA TN D-5492.

Nysmith, C. R., and J. L. Summers (1962). An experimental investigation of the impact resistance of double-sheet structures at velocities to 24,000 ft/s. NASA TN D-1431.

O'Neal, R. L. (1968). The Explorer 23 micrometeoroid satellite. NASA TN D-4284.

Posever, F. C., and C. N. Scully (1965). Investigation of meteoroid impacts on two-sheet configurations. AFFDL-TR-65-196. Wright-Patterson Air Force Base, Ohio.

Prater, R. F. (1970). Hypervelocity impact: material strength effects on crater formation and shock propagation in three aluminum alloys. ASML-TR-70295. Wright Patterson Air Force Base, Ohio.

Richardson, A. L. (1969). Theoretical penetration mechanics of multi-sheet structures based on discrete particle modeling. Paper Number 69-371, AIAA Hypervelocity Impact Conference, Vol. of Technical Papers.

Rinehart, J. S., and J. Pearson (1963). Explosive Working of Metals. The Macmillan Company, New York.

Riney, T. D. (1964). Theoretical hypervelocity impact calculations using the Pickwick code. R64SD13. GE Space Sciences Laboratory, Philadelphia.

Riney, T. D., and J. F. Heyda (1964). Hypervelocity impact calculations and their correlations with experiment. R64SD64. GE Space Sciences Laboratory, Philadelphia.

Rosen, F. D., and C. N. Scully (1965). Impact flash investigations to 15.4 km/s. In Proc. Seventh Hypervelocity Impact Symposium, Vol. 6. pp. 109-140.

Rosenblatt, M. (1970). Analytical study of strain rate effects in hypervelocity impacts. Final Report, Contract NAS8-20235.

Roy, N. L., J. C. Slattery, and J. F. Friichtenicht (1972). Study for Apollo meteoroid window experiment. Report Number 20921-6001-RO-00. TRW Systems, California.

Sawle, D. R. (1969). Hypervelocity impact in thin sheets and semi-infinite targets at 15 km/s. In Paper Number 69-368, AIAA Hypervelocity Impact Conference, Vol. of Technical Papers.

Scully, C. N., E. A. Escallier, F. D. Rosen, and J. D. O'Keefe (1965). The electrothermal gun for hypervelocity ballistics research. In Proc. Seventh Hypervelocity Impact Symposium, Vol. 1.

Sedgwick, R. T. (1969). Theoretical study of size scaling in cratering resulting from hypervelocity impact. Final Report, Contract NAS8-20239.

Slattery, J. C., and J. F. Friichtenicht (1966). Experimental research on hypervelocity cratering by microscopic particles. Report Number 03246-6001-RO-00, TRW Systems, California.

Sorensen, N. R. (1965). Systematic investigation of crater formation in metals. In Proc. Seventh Hypervelocity Impact Symposium, Vol. 6.

Swift, H. F. (1982). Hypervelocity impact mechanics. In Impact Dynamics, John Wiley, New York. pp. 215-230.

Swift, H. F., R. Bamford, and R. Chen (1982). Designing dual-plate shields--a new analysis. JPL Publication 82-39. Jet Propulsion Laboratory, California.

Swift, H. F., and A. K. Hopkins (1969). The effects of bumper material properties on the operation of spaced hypervelocity particle shields. Paper Number 69-379, AIAA Hypervelocity Impact Conference, Vol. of Technical Papers.

Swift, H. F., D. D. Preonas, W. C. Turpin, and J. H. Cunningham (1969). Characterization of debris clouds behind impacted meteoroid bumper plates. Paper Number 69-380, AIAA Hypervelocity Impact Conference, Vol. of Technical Papers.

Taff, L. G., D. E. Beatty, A. J. Yakutis, and P. M. Randall (1985). Low-altitude one centimeter space debris search at Lincoln Laboratory's (M.I.T.) experimental test system. In Space Debris, Asteroids and Satellite Orbits, Advances in Space Research, Vol. 5, Number 2. Pergamon Press, Oxford. pp. 34-45.

Teng, R. N. (1968). Hypervelocity impact damage in aluminum targets. DAC-59816. McDonnell-Douglas Aircraft Company, California.

Turpin, W. C., and J. M. Carson (1970). Hole growth in thin plates perforated by hypervelocity pellets. AFML-TR-70-83. Wright-Patterson Air Force Base, Ohio.

Wagner, M. H., N. B. Brooks, and R. L. Bjork (1965). Impact of a porous aluminum projectile on aluminum at 20 and 72 km/s. In Proc. Seventh Hypervelocity Impact Symposium, Vol. 3. pp. 1-54.

Walsh, J. M., and W. E. Johnson (1965). On the theory of hypervelocity impact. In Proc. Seventh Hypervelocity Impact Symposium, Vol. 2. pp. 1-75.

Walsh, J. M., W. E. Johnson, J. K. Dienes, J. H. Tillotson, and D. R. Yates (1964). Summary report on the theory of hypervelocity impact. GA-5119. General Atomic Division of General Dynamics, California.

Wenzel, A. B., and J. W. Gehring (1965). Hypervelocity impact studies against Apollo-type structures up to 16.5 km/s. TR65-56. GM Defense Research Laboratories, Santa Barbara, California.

Whipple, F. L. (1938). Photographic meteor studies: No. 1. Proc. Amer. Phil. Soc., 79 pp. 499-548.

Whipple, F. L. (1946). Possible hazards to satellite vehicle from meteorites. In The Collected Contributions of Fred L. Whipple, Vol. 2. Smithsonian Institution, Washington, D. C. pp. 1072-1079.

Whipple, F. L. (1952). Meteoritic phenomena and meteorites. In The Physics and Medicine of the Upper Atmosphere. University of New Mexico Press, Albuquerque. pp. 137-170.

Whipple, F. L. (1954). Photographic meteor orbits and their distribution in space. Astron. J., 59. pp. 201-217.

Whipple, F. L. (1958). The meteoric risk to space vehicles. In Proc. International Astronautical Congress. Springer-Verlag, Vienna. pp. 418-428.

Wilkinson, J. P. (1968). A penetration criterion for double-walled structures subject to meteoroid impact. 68SD275. GE Technical Center, Schenectady, New York.

Woodall, S. R. (1967). A numerical method for analyzing meteoroid two-sheet structural configuration impact problems. Mechanics Section Technical Memo 067-6A. GE Space Sciences Laboratory, Philadelphia.

Yew, C. H., and R. R. Kendrick (1986). A study of damage in composite panels produced by hypervelocity impact. In International J. Impact Eng., Vol. 5. Pergamon Press, Oxford.